PHYSICAL REVIEW C VOLUME 10, NUMBER 4 OCTOBER 1974

Refractive behavior in intermediate-energy alpha scattering*

D. A. Goldberg, S. M. Smith,† and G. F. Burdzik‡
Department of Physics and Astronomy, University of Maryland, College Park, Maryland 20742
(Received 10 June 1974)

We report on recent α-scattering experiments at 141.7 MeV using ^{40}Ca and ^{90}Zr targets. The results are compared with previous experiments on other nuclides at approximately the same energy and are used to illustrate phenomena occurring in intermediate-energy α scattering to which we have given the name "refractive behavior." All the elastic scattering differential cross sections exhibit the exponential-like falloff at large angles characteristic of *nuclear* rainbow scattering. The variation in the rainbow angle with A is found to be approximately linear. In each instance it is shown that, consistent with earlier predictions, it is the data beyond the rainbow angle which make possible the elimination of the discrete ambiguities in the optical potential: For each nucleus studied, only a single family of Woods-Saxon optical potentials is found to fit the data. The real parts of the extracted potentials are characterized by well depths ranging from 108 to 118 MeV and volume integrals $J/4A$ ranging from 297 to 352 MeV fm^3; hence they are more nearly three times the strength of nucleon-nucleus potentials at 1/4 the incident energy, rather than 4 times, as is frequently assumed. Systematic variations of the optical potentials with A occur primarily in the imaginary part of the potential and are greatest for the lighter nuclei; as A decreases, W and a' decrease, r_0' increases, and the volume integral of the real part of the potential increases.

[NUCLEAR REACTIONS ^{40}Ca, ^{90}Zr(α,α), $E=141.7$; enriched targets; measured $\sigma(\theta)$; deduced optical-model parameters, nuclear rainbow angles; results compared with those from ^{58}Ni, ^{12}C.]

I. INTRODUCTION

In a previous paper by two of the present authors,[1] criteria were presented for the incident energy and angular range of data necessary for the elimination of discrete ambiguities in optical potentials for composite projectiles. These criteria were based on a refractive description of nuclear scattering, preliminary accounts of which have appeared elsewhere.[2] Scattering phenomena to which this description is applicable we characterize as exhibiting "refractive behavior."

One of the most striking manifestations of refractive behavior occurs in the intermediate energy scattering of composite projectiles. Such scattering is characterized by the existence of a maximum deflection angle Θ_r, beyond which the differential cross section exhibits an almost exponential falloff.[1,2] The main purposes of the present paper are to provide additional illustrations of refractive behavior, to examine the A dependence of such behavior, and to perform additional tests of the criteria developed in Ref. 1. A secondary purpose is to study the A dependence of optical potentials for 140 MeV α particles.

The validity of the above criteria for data which permit resolution of discrete ambiguities (hereafter referred to as the "discrete-ambiguity criteria") was originally demonstrated[1] using the scattering data of 139 MeV α particles incident on ^{58}Ni. Predictions were made about the variation with target mass of both the energy and scattering-angle criteria, and the results of experiments involving the scattering of 139 MeV α particles by[3] ^{208}Pb and by[4] ^{12}C agreed with these predictions. It was felt that experimental data for a larger number of nuclei would be desirable, both to provide further tests of the discrete-ambiguity criteria and to permit a systematic study of refractive behavior. On both grounds, one would want data which, in each instance, extended beyond the maximum deflection angle Θ_r.

Existing sets of elastic α-scattering data at[5] 104 MeV and[6] 166 MeV appeared to be of limited use for such studies. Using the optical potentials given in Refs. 5 and 6 we calculated Θ_r for a number of the cases and found that for both sets of experiments, the only target nuclei for which data extended beyond their respective Θ_r were nuclei with $A < 28$. Since this would severely limit the scope of any study of mass systematics, we decided to proceed by extending our own 139 MeV experiments.[7]

In order to make further comparisons possible, we decided to choose as targets nuclei for which extensive elastic scattering data already existed for a variety of incident particles and bombarding energies. Based on model calculations, ^{90}Zr appeared to be the heaviest of such widely studied nuclei for which data exhibiting refractive behavior could be obtained with reasonable effort at an incident energy on the order of 140 MeV. The choice of ^{40}Ca as a second such widely studied nucleus was motivated by the fact that as the heaviest stable $T=0$ nucleus, it has been preferred[8] as a "calibration" nucleus for folding-model or "microscopic" optical-model calculations.

We begin our report with a brief outline of the refractive picture of nuclear scattering and a brief description of those characteristics which we refer to as refractive behavior. Following this we describe the present experiments. Results of the optical-model analysis of the present data are compared with those of previous experiments.[3,4] Finally we discuss the various aspects of refractive behavior illustrated by the data, with particular emphasis on the systematic A dependence of such behavior.

II. CHARACTERISTICS OF REFRACTIVE BEHAVIOR

At suitably high energies the quantum mechanical description of scattering can be formulated in the semiclassical or JWKB approximation.[9] If one regards the Schrödinger equation as a particle equation, then in the semiclassical limit the scattering description approaches that of classical mechanics and one speaks of trajectories and impact parameters; if one regards it as a wave equation, the description approaches that of geometrical optics and one speaks of indices of refraction. In our characterization of features of intermediate energy α scattering as refractive behavior, we borrow heavily on the results of both these interpretations. We have nonetheless chosen the term "refractive behavior" to indicate that "wave" effects may persist in this limit.

The wave-mechanical and particle descriptions are also connected in the semiclassical picture by associating a particle trajectory with each partial wave. The impact parameter b of the trajectory is related to the lth partial wave and the wave number k by

$$b=(l+\tfrac{1}{2})/k\,. \tag{1}$$

The particle's scattering angle (or more precisely, the classical deflection function) is thus related to the semiclassically calculated phase shift by

$$\Theta(l)=2\,\frac{d\delta_l}{dl}\,. \tag{2}$$

Here δ_l represents the *total* phase shift (e.g., in the case of charged particles, it includes the Coulomb phase shift). For repulsive potentials the $\Theta(l)$ are positive; for attractive potentials, negative.

Equation (2) is strictly correct only for a purely real potential. In nuclear scattering, however, a complex optical potential is used to account for the absorption of particles. No classical analog to such a potential exists in the expression for the classical deflection function. Nonetheless, if the imaginary part of the potential is small we can make the approximation that

$$\Theta(l)=2\,\frac{d(\mathrm{Re}[\delta_l])}{dl}\,, \tag{3}$$

where δ_l is now calculated semiclassically from the complex potential.

If one writes the Schrödinger equation for a complex potential as an optics equation involving a spatially varying complex refractive index, then the real part of the JWKB phase shift can be written as an integral of the real part of the index of refraction along the classical trajectory (see Appendix). Using Eq. (3) one can then relate this integral to the scattering behavior in a particular angular region. In classical optics, if one is able to relate the scattering (or deflection) into a given angular region to the real part of the index of refraction along a ray trajectory, one describes the scattering behavior in that region as refractive. When the analogous situation occurs in particle scattering, we likewise refer to it as refractive behavior.

We might note that the identification of a particular angular region with the real part of the index of refraction using the semiclassical interpretation rests on the validity of Eq. (3). This equation requires not merely that the energy be sufficiently high that JWKB be valid, but also that the imaginary part of the complex potential be small relative to the real part, i.e., that the real part of the refractive index depends primarily on the real part of the potential. Hence one indication that a feature of the cross section exhibits refractive behavior is that its angular variation depends primarily on the real part of the potential.

As mentioned in the Introduction, one of the most striking manifestations of refractive behavior occurs in the intermediate energy scattering of composite projectiles. For such scattering $\Theta(l)$ has a maximum value less than 180°, defined previously as Θ_r, beyond which the cross section exhibits an almost exponential falloff.

An illustration of such behavior, which also illustrates that it is dependent only on the real part of the potential, is given in Fig. 1. The calculated value of Θ_r for the potential used is approximately 62°, and one sees clearly the exponential-like falloff of the cross section beyond Θ_r. Moreover, one sees from the various model calculations, in which the imaginary part of the potential W is reduced in 5 MeV steps to zero, that the falloff results from

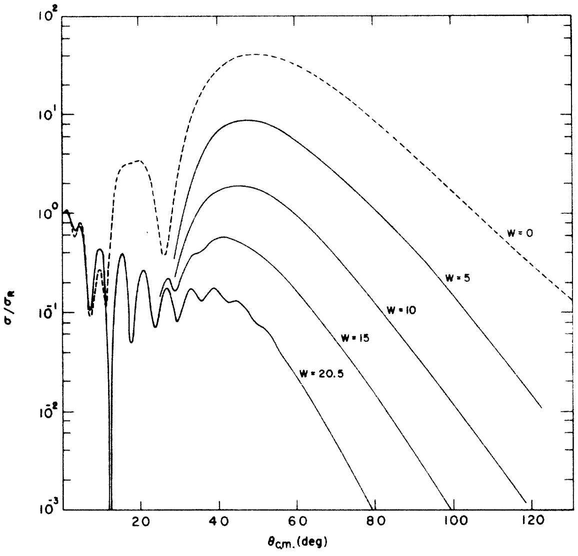

FIG. 1. Calculations of the differential cross section for the elastic scattering of 139 MeV α particles from ^{58}Ni. The curve labeled $W=20.5$ represents the actual fit to elastic scattering data obtained in Ref. 3. The other curves represent model calculations made using different strengths (W) for the imaginary part of the potential, but with the same real potential. Changing W changes only the magnitude of the cross section at large angles but leaves the shape unaffected.

the real potential alone; changing W affects only the *magnitude*, not the *shape*, of the cross section beyond Θ_r.[10] The fact that the cross section does not vanish abruptly at Θ_r is, of course, due to non-ray-like wave effects[11]; we nonetheless characterize the falloff as "refractive" behavior since the existence and location of the maximum deflection angle are determined by the real part of the nuclear refractive index.[12]

The phenomenon of a maximum deflection angle is discussed extensively in Ref. 9, where the authors refer to Θ_r as the rainbow angle. In the case they consider, which also involves scattering of α particles by nuclei, the maximum deflection angle occurs for impact parameters in the region of the outer nuclear surface at the point at which the attractive nuclear force begins to overcome Coulomb repulsion. Such *Coulomb* rainbow scattering is therefore characterized by a positive Θ_r, or *Coulomb* rainbow angle. In the case discussed in the present paper, the Θ_r referred to is the maximum *negative* deflection angle produced by the attractive nuclear potential. At intermediate energies this *nuclear* rainbow angle is generally much larger than the Coulomb rainbow angle and so Coulomb rainbow scattering is generally not observed. The importance of nuclear rainbow scattering in removing discrete ambiguities from composite-projectile optical potentials was originally demonstrated in Ref. 1. Additional illustrations of the effect are presented in the present work.

III. PRESENT EXPERIMENT

The experimental procedures were essentially the same as those described in Ref. 3, although the present experiments employed several improvements and modifications in technique. For forward angle measurements a detector aperture of nominally $\frac{1}{4}°$ horizontal by $1°$ vertical was employed. The horizontal size of the beam spot was set equal to the detector slit width and the horizontal divergence of the beam was $\pm\frac{1}{8}°$, so that the over-all angular resolution was on the order of $\frac{1}{2}°$. At the larger angles, a detector aperture of nominally $\frac{1}{2}°$ horizontal by $1.35°$ vertical was used. The accuracy of the measured angular position of the detectors was $\pm 0.02°$. Determinations of the zero angle of the beam made before and after each set of measurements indicated an additional error due to (drift + uncertainty) of $\pm 0.02°$. Accordingly, the error bars assigned to the data points reflect an angular uncertainty of $\pm 0.03°$ (see Ref. 3).

The targets used in the present experiments were natural Ca (96% ^{40}Ca) and ^{90}Zr (99% enriched). The target thicknesses were (2.1 ± 0.1) mg/cm^2 and (5.9 ± 0.1) mg/cm^2, respectively.

Using the technique described in Ref. 3 we determined the beam energy to be 141.7 ± 0.2 MeV.[13] At forward angles the observed energy resolution was about 200 keV for the Ca target and 220 keV for Zr; roughly 150 keV of this was attributable to the beam. At larger angles the resolution worsened by about a factor of 2 as a result of the required increase in beam intensity, part of the effect being due to increasing the analyzing slit width and part to pileup caused by low energy particles.

The present data were normalized to the current integrator (Faraday cup) rather than to the monitor counter; the (dead time corrected) ratio of monitor to integrator counts remained constant to within the limit of statistical uncertainty. The error bars assigned to the individual data points reflect, in addition to the angular uncertainties noted earlier, the statistical uncertainties, augmented by uncertainties involved in defining the limits of the peaks and/or the background, these latter uncertainties being on the order of 1% or less.

The data were analyzed conventionally using the optical-model search code[14] JIB3 (modified to permit the use of up to 100 partial waves). We employed a six-parameter Woods-Saxon potential of the form

$$U(r) = -Vf(x) - iWf(x') + V_c(r),$$

where $f(x) = (1+e^x)^{-1}$, $x = (r - r_0 A^{1/3})/a$, $x' = (r - r_0' A^{1/3})/a'$, and V_c is the electrostatic potential of a uniformly charged sphere of radius $r_c A^{1/3}$. The parameters were determined by fitting the data to minimize the quantity

$$\chi^2 = \sum_{i=1}^{n} \{[\sigma_{th}(\theta_i) - \sigma_{exp}(\theta_i)]/\Delta\sigma(\theta_i)\}^2 .$$

The determination of the relative errors $\Delta\sigma(\theta_i)$ was described above.

The data from the present experiment are shown in Fig. 2 along with the optical-model "best fits." The characteristic falloff of the cross section at large angles is clearly evident in both sets of data, and, in agreement with the predictions of Ref. 1, we found only a single family of optical potentials which were able to fit the data. The parameters for these potentials, along with comparisons with previous results, are presented in the following section; we merely note here that in both instances the real well depths range from 108 to 118 MeV, and the volume integrals per projectile-target nucleon pair $J/4A$ are on the order of 300 MeV fm^3. Based on our earlier results,[3] it was not felt necessary to perform extensive grid searches on the parameters. However, following the procedure in Ref. 1 we were able in both cases to find a potential of well depth $V \simeq 170$ MeV which would fit the data only out to the rainbow angle Θ_r. This is discussed at greater length in Sec. V.

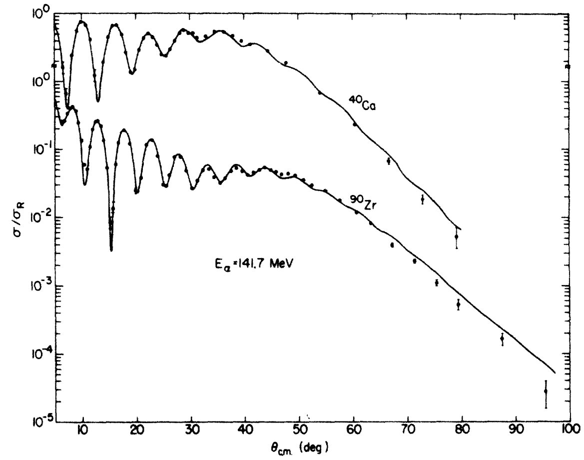

FIG. 2. Differential cross sections for elastic scattering of 141.7 MeV α particles from ^{40}Ca and ^{90}Zr. Solid curves represent optical-model fits to the data.

IV. COMPARISON OF OPTICAL POTENTIALS

We begin our discussion by examining the A dependence of the optical-potential parameters obtained from the analysis of elastic α scattering from four targets of differing mass, ^{12}C, ^{40}Ca, ^{58}Ni, and ^{90}Zr, at essentially the same incident (lab) energy. Since for a given nuclide the variations in the real-well strengths with energy for α particles in this energy range are typically[4,15] $\leq 0.5\%$ MeV^{-1}, we regard the effect of the difference in incident energy for the two groups of experiments as relatively insignificant.

The optical-potential parameters are given in Table I. For the real potentials $J/4A$, the volume integral per projectile-target nucleon pair, increases with decreasing A; r_0 appears to vary but not in any systematic way; V increases slightly with A, and a varies hardly at all. More pronounced systematic variations with target mass occur in the imaginary potential (with which we are only secondarily concerned) in the increase in a' and W, and the decrease in r_0' with increasing A.

To see to what extent the above variations might simply reflect (continuous) ambiguities in the optical-model fits, we tried adjusting some of the more "variant" parameters in the ^{12}C and ^{40}Ca potentials to more typical values and refitting the

TABLE I. Optical-model parameters. The form of the optical potential is a six-parameter Woods-Saxon well, as described in the text. The last two columns list respectively the values of χ^2 per degree of freedom obtained in fitting the data, and the volume integral per projectile-target nucleon pair for the real part of the potential.

Isotope	V (MeV)	r_0 (fm)	a (fm)	W (MeV)	r_0' (fm)	a' (fm)	r_0^c (fm)	χ^2/F	$J/4A$
^{12}C	108.0	1.215	0.760	16.99	1.846	0.468	1.26	4.2	353
^{40}Ca	107.8	1.315	0.763	19.76	1.694	0.514	1.30	2.8	329
^{58}Ni [a]	118.2	1.240	0.796	20.47	1.595	0.571	1.30	6.2	300
^{90}Zr	117.5	1.267	0.783	21.02	1.564	0.569	1.30	7.4	297

[a] The parameters quoted here differ slightly ($\leq$1.5%) from those of Ref. 3; this results from a change of r_0^c from 1.4 to 1.3 fm for purposes of comparison with the other nuclides.

data. In general, we found that adjusting the real-well parameters had little effect on those of the imaginary well, and vice versa; also, for both real and imaginary wells an increase in radius was correlated with a decrease in well depth and diffuseness, regardless of which parameter was actually being adjusted.

The results of trying to bring the variant parameters "into line" were as follows: For ^{40}Ca, reducing r_0' to 1.6 increased χ^2 fivefold and reducing a' to 0.57 doubled χ^2; reducing r_0 to 1.25 fm trebled χ^2. For ^{12}C, reducing r_0' to 1.70 fm increased χ^2 by 150%. However, increasing r_0 to 1.25 left χ^2 almost unaffected and increasing it to 1.3 (to bring it "in line" with ^{40}Ca) only increased χ^2 by about 20%; the latter change is accompanied by a reduction of V to about 98 MeV, and in a to 0.73. It should be observed that the increased "variability" of the ^{12}C parameters relative to those of ^{40}Ca is probably at least partly due to the improved quality (and hence smaller error bars) of the ^{40}Ca data, as described in Sec. III.

From the above, we would conclude that the trends in the imaginary part of the potential are "real," since attempts at suppressing the variations for the lighter nuclei result in considerably poorer over-all fits. The situation is less clear in the case of r_0, where there appears to be a variation, but no systematic trend. On the other hand, the variation of $J/4A$ with A appears to be monotonic and regular; moreover it has been demonstrated[16] that this quantity is quite insensitive to parameter variations due to continuous ambiguities. Finally, we note what is perhaps obvious, namely, that the marked variations seem to occur in the lighter nuclides, most particularly ^{12}C, i.e., in the region where one might expect the concept of a "nucleus" (as opposed to a bound system of a small number of particles) to begin breaking down.

More noteworthy than the variations, we feel, are the actual values of the strengths of the real part of the nuclear potentials, as measured in terms of either the well depths or volume integrals. The conventional wisdom is that the well depth for an α particle at incident energy E should be roughly 4 times that for a nucleon at energy $E/4$, and that the volume integral per projectile-target nucleon pair should therefore be the same for the two projectiles. Estimating the nucleon values from proton scattering data at 30 and 40 MeV,[17,18] we find that the predicted α-particle well depths are $V \gtrsim 180$ MeV and the values for $J/4A$ are roughly 390 MeV fm^3. Comparing these values with those in Table I, we see that the volume integrals are low by 20–25%, and the well depths are low by almost 40%, i.e., they are more nearly $2\frac{1}{2}$ times, rather than 4 times, the nucleon well depth.[19] These results are consistent with those of previous[5,6,20] intermediate energy α-scattering experiments.[21] The discrepancies are even greater if one takes into account the effect of the α-particle binding energy by reducing the effective incident energy of the nucleons within the α particle, since the energy dependence of the nucleon-nucleus potential is negative.

The question of a reduced α-particle well depth has been examined by several authors. Using arguments based on an energy-independent potential, Duhm[20] showed that using the $V_\alpha = 4V_N$ prescription is tantamount, in a bound-state calculation, to regarding the α particle separation energy as 4 times the nucleon separation energy; in turn, calculating the well depth from the observed α separation energy he found the well depth to be more nearly 3 times the nucleon well depth.

More recently, Jackson and Johnson[22] have examined the problem by folding nonlocal nucleon-nucleus potentials to get composite-projectile optical potentials. They find that the finite projectile size results in a reduced well depth, although for α particles, they estimate the reduction to be more like 15% rather than the presently observed 25%.

V. MASS SYSTEMATICS OF REFRACTIVE BEHAVIOR

In this section we consider the mass systematics of refractive behavior by comparing the results of elastic α-scattering experiments performed on four targets of differing mass, ^{12}C, ^{40}Ca, ^{58}Ni, and ^{90}Zr, at essentially the same incident energy. We begin in a qualitative way, namely, by comparing the shapes of the different angular distributions, which are shown in Fig. 3.

The most readily apparent aspect of the figure is the similarity of the over-all shapes of the cross sections, the small-angle diffraction oscillations in each case giving way to the exponential-like falloff at larger angles. The appearance of slight oscillations in the falloff region is essentially due to superposition of the absorptive diffraction scattering and the refractive rainbow scattering. The strength of the interference is dependent on the damping of the diffraction oscillations which increases with the diffuseness of the strongly absorbing nuclear disk, i.e., with a'. Examination of the parameters in Table I shows that the lighter nuclei have the smaller a', i.e., the least damping; this is consistent with the observed variation with A of the amplitude of the oscillations in the rainbow region.

This increased persistence of diffraction oscil-

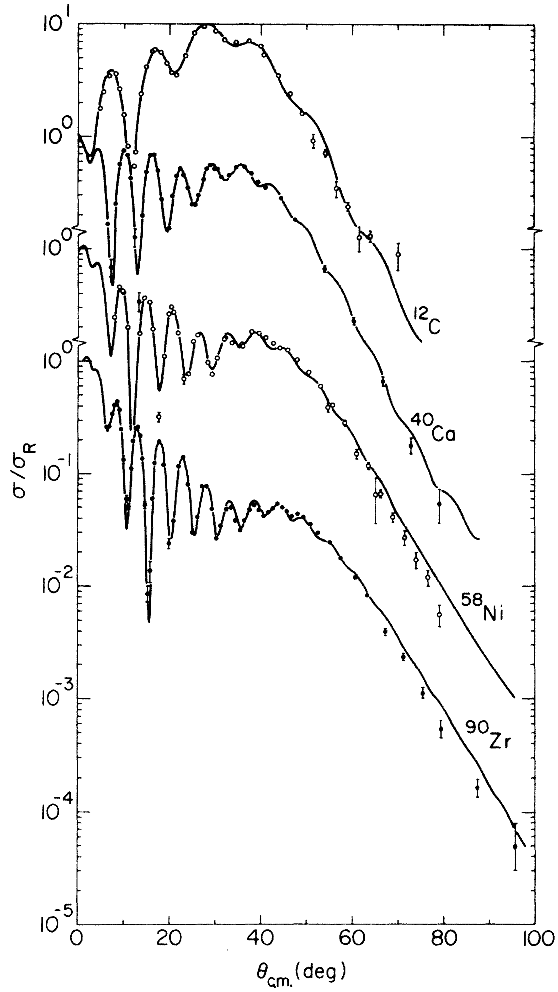

FIG. 3. Comparison of differential cross sections for elastic scattering of α particles ($E_\alpha \simeq 140$ MeV) from a variety of nuclei. Solid curves represent optical-model fits to the data using the parameters given in Table I in the text.

lations for the lighter nuclei tends to mask another systematic trend, the shift of the onset of the falloff region to larger angles with increasing A. This shift of the falloff region with A is simply a reflection of the increase in the rainbow angle Θ_r with A. This shift can be understood as follows. We have shown previously[3] that ϵ_{crit}, the minimum center of mass bombarding energy for which orbiting or spiral scattering ceases, and above which rainbow scattering occurs, increases with increasing A; we used the specific comparison of ^{58}Ni and ^{208}Pb nuclei both to illustrate the origin and demonstrate the validity of this result. Moreover, it is readily apparent that the maximum deflection angle for a given nucleus decreases with bombarding energy. An incident energy which is only slightly greater than ϵ_{crit} for a large-A nucleus, will be well above ϵ_{crit} for a small-A nucleus, and hence will result in a smaller value of Θ_r for the latter than the former. Hence at a given bombarding energy one expects the falloff region to begin at smaller angles for lighter nuclei, consistent with the results in Fig. 3.

We can demonstrate the above quantitatively by calculating the semiclassical deflection function $\Theta(l)$ for each of the cases shown in Fig. 3. The results of these calculations are shown in Fig. 4, where we have plotted the deflection functions as a function of impact parameter $b=(l+\frac{1}{2})/k$ rather than l [i.e., we plot $\Theta(b)$ rather than $\Theta(l)$].[23] One immediately verifies that Θ_r, the maximum (absolute) value of $\Theta(b)$ indeed increases with A. Semiclassically one expects that the maximum deflection angle would correspond to a trajectory roughly tangent to the nuclear surface, where the nuclear force is greatest. One then expects that b_r, the impact parameter corresponding to Θ_r, should increase with increasing A, as is shown to be the case in Fig. 4.

We might note almost in passing another feature illustrated in Fig. 4. We referred in Sec. II to the existence of both a nuclear and a Coulomb rainbow angle. The latter corresponds to the maximum *positive* value of $\Theta(b)$ which, as may be seen in Fig. 4, occurs for a considerably larger impact parameter, and smaller angle, than the corresponding nuclear rainbow angle. Also, as expected, the Coulomb rainbow angles are seen to be larger for the more strongly charged high-A nuclei.

Returning to the variation of Θ_r with A, we have examined the matter further by plotting Θ_r as a

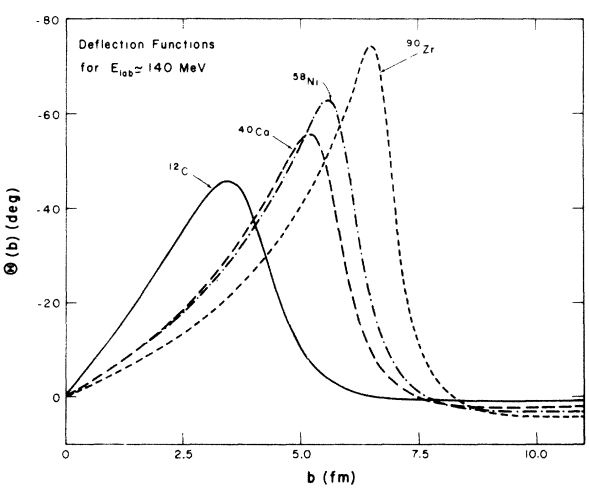

FIG. 4. Semiclassical deflection functions for the scattering of 140 MeV α particles from various nuclei. The deflection functions are here plotted as a function of impact parameter $b=(l+\frac{1}{2})/k$ rather than l.

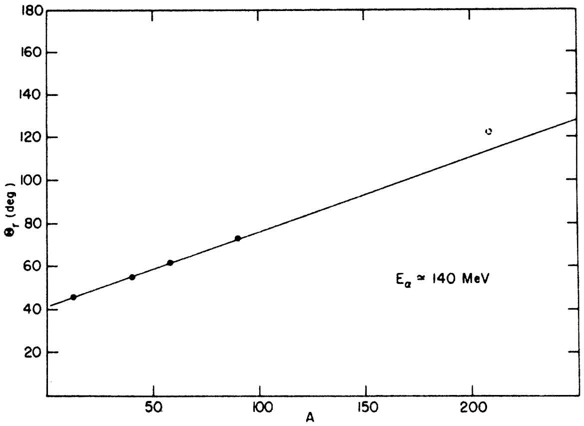

FIG. 5. Maximum deflection (rainbow) angle for scattering of 140 MeV α particles as a function of target mass. Point corresponding to ^{208}Pb is shown "dashed" due to inadequacy of scattering data (see text).

function of A, as shown in Fig. 5, based on the calculations for Fig. 4. From Fig. 5, it appears that the relation between Θ_r and A is approximately linear. We have actually indicated a fifth "datum" in the plot, the value of Θ_r for 139 MeV α particles on ^{208}Pb as calculated from potential 1 in Ref. 3. We have indicated this point as a "dashed" point, since the data on which it is based did not extend to the calculated Θ_r; not only does

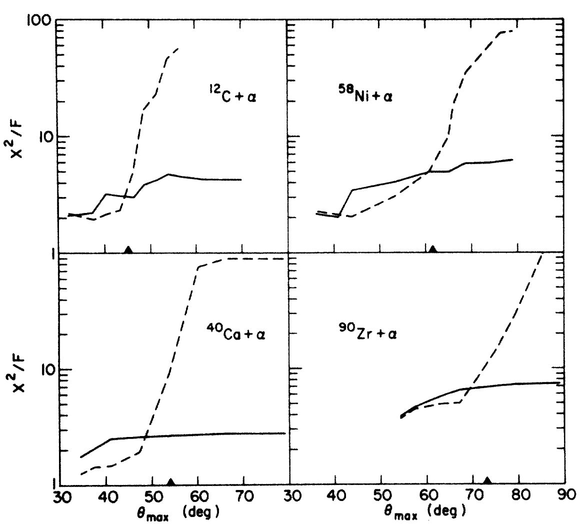

FIG. 6. χ^2/F for best fits to subsets of full scattering data obtained by truncating the data at $\theta=\theta_{max}$, plotted as a function of θ_{max}. The solid curves are for the so-called shallow potentials ($V\simeq 115$ MeV); the dashed curves, the so-called deep potentials ($V\simeq 170$ MeV). The calculated value of the nuclear rainbow angle Θ_r for each nucleus is indicated by the heavy triangle. In each case as θ_{max} is increased beyond Θ_r, the χ^2/F for the deep potential rises abruptly, whereas that for the shallow potential remains essentially unchanged.

this indicate that the data were insufficient to permit unambiguous determination of the correct optical-model family for ^{208}Pb, but that even within the family, the parameters may be inadequately defined. In any event, the increase of Θ_r with A is supported by the ^{208}Pb datum[24]; moreover, the plot appears to indicate that the empirical linear relationship provides a good approximation to Θ_r for virtually the entire range of A.

Having demonstrated the manifestations of refractive behavior in the elastic scattering cross sections, we now turn our attention to what seems to us the most significant consequence of that behavior, namely, that the data beyond the rainbow angle Θ_r make possible elimination of discrete ambiguities in the optical potential. In Ref. 1 we illustrated this using the ^{58}Ni data. We did this by fitting subsets of the data, which were obtained by truncating the full data at various angles θ_{max}, and searching on the optical-model parameters to minimize χ^2. For θ_{max} less than Θ_r, in addition to the potentials with $V\simeq 115$ MeV, we found a second so-called "family" in the neighborhood of $V\simeq 170$ MeV which gave comparable χ^2. However, as we increased θ_{max} beyond Θ_r, the χ^2 for the deeper family rose abruptly, whereas that for the shallow family remained essentially unchanged. We have now repeated that procedure using the ^{12}C, ^{40}Ca, and ^{90}Zr data; the results are shown in Fig. 6. As noted earlier, in each case we were able to find a "deep" family. As may be seen from Fig. 6, in each case as θ_{max} increases beyond Θ_r, the χ^2 for the deeper potential rises abruptly, where-

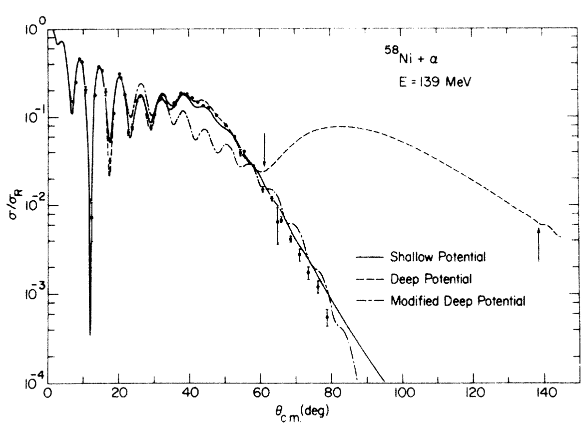

FIG. 7. Comparison of cross sections for elastic scattering of 139 MeV α particles from ^{58}Ni predicted by the shallow and deep potentials. The deep potential was obtained by fitting the data out to 61°. The arrows indicate the respective maximum deflection angles calculated using the shallow and deep potentials. The curve denoted as "modified deep potential" is described in the text.

as that for the shallow potential remains essentially unchanged.

The difference between the two potentials (and the total inadequacy of the deeper one) is clearly demonstrated in Fig. 7, where one sees that at the rainbow angle (indicated by the downward arrow) the cross section for the deep family rises rather dramatically relative to that of the shallow family, the latter continuing to follow the exponential-like falloff of the data. The semiclassically calculated rainbow angle for the deeper potential, indicated by the upward arrow, occurs at a much larger angle than that for the shallow potential; hence the cross section for the deep potential does not begin its exponential-like falloff until much larger angles. The illustration here is for the ^{58}Ni potentials; similar results are obtained for the other nuclides.

One additional point is worth noting. The potential referred to in Fig. 7 as the "deep potential" is the one obtained by fitting the data to $\theta_{max} = \Theta_r$. This is consistent with its representing a "continuation" of the deep potential obtained at lower energies, where of course *all* data are forward of the rainbow angle. To try to overcome the peaking beyond the rainbow angle, one can try to fit the full set of data with a deep potential having a stronger absorptive part. Such a fit is shown in Fig. 7, labeled as "modified deep potential." However, such a potential is not representative of a discrete ambiguity, since it does not fit the forward angle data at all well and its real-well parameters differ from those of the "continued" deep potential. (The abrupt flattening out of the χ^2/F vs θ_{max} curves for ^{40}Ca and ^{58}Ni in Fig. 5 indicates the point at which the "best fit" for the deep well changes over from the "continued" deep family to the strongly absorbing one.) Moreover, no such strongly absorbing potential with anything resembling reasonable geometric parameters, i.e., $r_0 > 0.9$ fm, could be found for ^{12}C.

VI. CONCLUSIONS

We have compared the results of the present α-scattering experiments using ^{40}Ca and ^{90}Zr targets with those of previous experiments at essentially the same incident energy using ^{58}Ni and ^{12}C targets. In all four cases the differential cross sections exhibited the falloff at large angles which is characteristic of *nuclear* rainbow scattering and which, due to its dependence on the *real* part of the nuclear index of refraction, we characterize as refractive behavior. For each nuclide studied, a unique family of Woods-Saxon optical potentials was obtained by fitting the data, consistent with the predictions of Ref. 1. Moreover, following the procedures described in Ref. 1, we have shown that in each case it is indeed the data beyond the *nuclear* rainbow angle Θ_r that make possible the elimination of the discrete ambiguity. We also note that the refractive picture correctly predicts the increase in Θ_r and b_r with target mass, the former quantity empirically being found to vary linearly with A.

A comparison of optical potentials obtained by fitting the data reveals that for such systematic A dependences as exist in the optical-model parameters, the variations are most pronounced for the lighter nuclei. For the imaginary part of the potential we find that as A decreases W and a' decrease and r_0' increases. In the real part of the potential, the only strong trend is an increase of the volume integral $J/4A$ with decreasing A, although V also appears to decrease slightly.

More significant than the variation of the real potential with A is the actual well strength. Comparing with the common prescription that the well strength for incident particles of energy E should be four times that of nucleons at energy $E/4$, we find that the well depths are 30–40% low and, except for ^{12}C, the volume integrals are $\simeq$ 20–25% low. As noted in the text, these results are consistent with those of other intermediate energy α-scattering experiments. Explanations for the reduced α-well strength basically attribute it to the tight binding of the nucleons in the α particle (as manifested in either reduced α-separation energies or the small size of the α); in some sense there is a saturation of the forces of the α-particle nucleons and hence a reduction of their external interaction.

A final comment on optical-potential ambiguities. In the past there have been various attempts to resolve the discrete ambiguity by examining fine details of the differential cross sections, e.g., deep minima, and seeing which optical-model family best reproduces them. To compare the appropriateness of this type of approach with that of the procedure given in Ref. 1 and the present paper, we might consider the case of the deep minimum in the ^{58}Ni data at $\theta \simeq 20°$ (see Fig. 6). We note that the deep potential, which fails utterly to fit the data beyond the rainbow angle, fits that particular minimum quite well, appreciably better than does the shallow potential, which we now know to be (within the constraint of the six-parameter Woods-Saxon optical model) the correct one. (We have observed similar occurrences in both the ^{40}Ca and ^{90}Zr data as well.) We would submit that examination of fine details of cross sections, rather than providing grounds for discriminating among various Woods-Saxon wells, in fact reveals the deficiencies of the Woods-Saxon form of the optical potential.

ACKNOWLEDGMENTS

The excellent beam quality in the present experiment was largely due to the assistance of R. E. Berg in setting up both the cyclotron and beam transport system prior to the run. The task of data taking during the run was made considerably easier with the help of J. N. Craig, K. Kwiatkowski, and C. C. Chang, as well as that of Carl Peridier, who also assisted in the preliminary analysis of the data. Our continuing debt to N. R. Yoder for his assistance with the data acquisition code GELIAN and the data analyzing procedure is gratefully acknowledged. We would also like to express our thanks to the entire staff of the University of Maryland cyclotron. The stay at the University of Maryland by one of the authors (G. F. B.) was made possible by a travel grant from Council for Scientific Industrial Research.

APPENDIX

We can write the radial part of the Schrödinger equation in the form of an optics wave equation

$$\frac{d^2\psi_l(r)}{dr^2}+[kn_l(r)]^2\psi_l(r)=0\,. \tag{A1}$$

The local index of refraction is then defined as

$$\mathrm{Re}[n_l(r)]=\frac{1}{\sqrt{2}}\{[(1-V_{\mathrm{eff}}/E)^2+(W/E)^2]^{1/2}+(1-V_{\mathrm{eff}}/E)\}^{1/2}\,, \tag{A2a}$$

$$\mathrm{Im}[n_l(r)]=\frac{1}{\sqrt{2}}\{[(1-V_{\mathrm{eff}}/E)^2+(W/E)^2]^{1/2}-(1-V_{\mathrm{eff}}/E)\}^{1/2}\,, \tag{A2b}$$

where the complex optical potential is written as

$$U(r)=V(r)+i\,W(r)$$

and

$$V_{\mathrm{eff}}=V_{\mathrm{eff}}(l,r)=[\hbar^2(l+\tfrac{1}{2})^2]/\,2\mu r^2+V(r)+V_c(r).$$

Following Ref. 9, one can write the phase shifts as

$$\delta_l=\lim_{R\to\infty}\left(k\int_{r_2}^{R}\{1-[\hbar^2(l+\tfrac{1}{2})^2/2\mu r^2+U(r)+V_c(r)]/E\}^{1/2}dr-k\int_{r_1}^{R}[1-(l+\tfrac{1}{2})^2/k^2r^2-2\eta/kr]^{1/2}dr\right), \tag{A3}$$

where for the purposes of calculating $\Theta(l)$, r_2 and r_1 are the classical turning points in the presence and absence, respectively, of the nuclear plus finite-size Coulomb potentials and are defined by the relations

$$1-[\hbar^2(l+\tfrac{1}{2})^2/2\mu r_2^{\,2}+V(r_2)+V_c(r_2)]/E=0\,, \tag{A4a}$$

$$1-(l+\tfrac{1}{2})^2/k^2r_1^{\,2}-2\eta/kr_1=0\,, \tag{A4b}$$

where η is the Sommerfeld parameter, and $k=(2mE)^{1/2}/\hbar$.

We can write (A3) in terms of the refractive indices $n_l(r)$ as

$$\mathrm{Re}[\delta_l]=\lim_{R\to\infty}\left\{k\int_{r_2}^{R}\mathrm{Re}[n_l(r)]\,dr-\int_{r_1}^{R}K_l(r)dr\right\} \tag{A5a}$$

$$\mathrm{Im}[\delta_l]=\lim_{R\to\infty}\left\{k\int_{r_2}^{R}\mathrm{Im}[n_l(r)]\,dr\right\}, \tag{A5b}$$

where

$$K_l(r)=k[1-(l+\tfrac{1}{2})^2/k^2r^2-2\eta/kr]^{1/2}\,.$$

From (A5a) we see that $\mathrm{Re}[\delta_l]$ only depends on the real part of the refractive index (plus a term which is independent of the potential). Moreover, in the event that $V_{\mathrm{eff}}/E \gg W/E$, we see from (A2a) that $\mathrm{Re}[n_l]$ is primarily dependent on the real part of the potential and $\mathrm{Re}[\delta_l]$ approaches the value which would obtain for a purely real potential.

*Work supported in part by the U. S. Atomic Energy Commission.

†Present address: Education and Public Affairs, Washington, D. C.

‡Permanent address: Council for Scientific Industrial Research, Pretoria, South Africa.

[1]D. A. Goldberg and S. M. Smith, Phys. Rev. Lett. 29, 500 (1972).

[2]S. M. Smith and D. A. Goldberg, Bull. Am. Phys. Soc. 17, 591 (1972); University of Maryland Progress Report 1972 (unpublished).

[3]D. A. Goldberg, S. M. Smith, H. G. Pugh, P. G. Roos, and N. S. Wall, Phys. Rev. C 7, 1938 (1973).

[4]S. M. Smith *et al.*, Nucl. Phys. A207, 273 (1973).

[5]G. Hauser, R. Löhken, H. Rebel, G. Schatz, G. W. Schweimer, and J. Specht, Nucl. Phys. A128, 81 (1969); H. Rebel *et al.*, *ibid.* A182, 145 (1972).

[6]I. Brissaud, M. K. Brussel, M. Sowinski, and B. Tatischeff, Phys. Lett. 30B, 325 (1969); B. Tatischeff and I. Brissaud, Nucl. Phys. A155, 89 (1970).

[7]We should note that our own ^{208}Pb data also suffered from the defect of inadequate angular range, and for this reason we have in most instances excluded ^{208}Pb results from the present study.

[8]A. M. Bernstein and W. A. Seidler, Phys. Lett. 39B, 583 (1972).

[9]K. W. Ford and J. A. Wheeler, Ann. Phys. (N. Y.) 7, 259, 287 (1959).

[10]It should be noted that the mere existence of a falloff in the cross section at large angles is not in and of itself evidence of rainbow scattering. However, short of a complete semiclassical phase shift calculation, a simple test for the existence of rainbow scattering can be made by performing the sort of model calculations illustrated in Fig. 1; if the shape of the falloff is independent of the strength of the absorption, then rainbow scattering is occurring.

[11]This illustrates the remark made earlier about relative aptness of the geometrical optics and classical particle limits. In the limit given by the optical analog, one might still expect illumination of the region forbidden by geometrical optics, such as occurs in Fresnel diffraction.

[12]It is worth noting that one does not observe such a region of monotonic falloff in nucleon-nucleus scattering. The reason for its absence is that refractive behavior requires that the real part of the nuclear refractive index be primarily dependent on the real part of the nuclear potential. For composite projectiles, where the real part of the optial potential is much larger than the imaginary part, this is the case; for nucleon optical potentials, with their relatively shallow real-well depths, it is not.

[13]The change in energy from experiments described in Refs. 3 and 4 is due to the repositioning of the electrostatic deflector in the cyclotron; the resulting energy difference was not deemed significant enough for the proposed comparisons to warrant correction (see Sec. IV of text).

[14]F. Perey, private communication.

[15]L. W. Put and A. M. J. Paans, Phys. Lett. 49B, 266 (1974).

[16]D. C. Weisser, J. S. Lilley, R. K. Hobbie, and G. W. Greenlees, Phys. Rev. C 2, 544 (1970).

[17]G. W. Greenlees and G. J. Pyle, Phys. Rev. 49, 836 (1966).

[18]L. N. Blumberg, E. E. Gross, A. van der Woude, A. Zucker, and R. H. Bassel, Phys. Rev. 147, 812 (1966).

[19]The volume integral for ^{12}C is actually more like 10% low. On the other hand, as noted in our earlier discussion of possible ambiguities in the parameters, the real-well depth for ^{12}C might well be even lower than the value quoted in Table I.

[20]H. H. Duhm, Nucl. Phys. A118, 563 (1968).

[21]As noted in the Introduction, many of these earlier results, primarily those for heavier nuclei, are based on data which do not fulfill the criteria of Ref. 1, although the quoted potentials are consistent with unambiguous results for higher energies or lighter nuclei. To make the present comparisons as definitive as possible, we have, as noted earlier, excluded our own results for ^{208}Pb, which are based on similarly "inadequate" data.

[22]D. F. Jackson and R. C. Johnson, Phys. Lett. 49B, 249 (1974).

[23]The plot in Fig. 4 is also inverted from the conventional form, i.e., we plot $-\Theta(b)$ rather than $\Theta(b)$.

[24]The argument of Ref. 1 concerning the increase of ϵ_{crit} with A was based on the various nuclei having similar parameters; potential 1, referred to in the text, is the potential most similar to those of the other four nuclei.